A conditioned level-set method with block-division strategy to flame front extraction based on OH-PLIF measurements

Han Yue(韩 乐)[a)†], Cai Guo-Biao(蔡国飙)[a)], Xu Xu(徐 旭)[a)], Renou Bruno[b)], and Boukhalfa Abdelkrim[b)]

[a)] *School of Astronautics, Beijing University of Aeronautics and Astronautics, Beijing* 100191, *China*

[b)] *UMR* 6614 *CORIA, INSA de Rouen, Avenue de l'Université, BP* 08, 76801 *Saint-Etienne du Rouvray, France*

(Received 30 November 2013; revised manuscript received 25 January 2014; published online 1 April 2014)

A novel approach to extract flame fronts, which is called the conditioned level-set method with block division (CLSB), has been developed. Based on a two-phase level-set formulation, the conditioned initialization and region-lock optimization appear to be beneficial to improve the efficiency and accuracy of the flame contour identification. The original block-division strategy enables the approach to be unsupervised by calculating local self-adaptive threshold values autonomously before binarization. The CLSB approach has been applied to deal with a large set of experimental data involving swirl-stabilized premixed combustion in diluted regimes operating at atmospheric pressures. The OH-PLIF measurements have been carried out in this framework. The resulting images are, thus, featured by lower signal-to-noise ratios (SNRs) than the ideal image; relatively complex flame structures lead to significant non-uniformity in the OH signal intensity; and, the magnitude of the maximum OH gradient observed along the flame front can also vary depending on flow or local stoichiometry. Compared with other conventional edge detection operators, the CLSB method demonstrates a good ability to deal with the OH-PLIF images at low SNR and with the presence of a multiple scales of both OH intensity and OH gradient. The robustness to noise sensitivity and intensity inhomogeneity has been evaluated throughout a range of experimental images of diluted flames, as well as against a circle test as Ground Truth (GT).

Keywords: OH-PLIF, flame front extraction, level-set, optical signal processing

PACS: 89.20.–a, 89.20.Ff, 42.62.–b, 42.62.Eh **DOI:** 10.1088/1674-1056/23/5/058901

1. Introduction

Since the introduction of various laser diagnostic techniques in combustion research and development, quantitative laser-based sensing has played an increasingly important role in deepening the understanding of the combustion processes.[1,2] Thanks to their non-intrusive features, laser techniques are able to provide reliable information about relevant parameters, such as temperature, species concentration, velocity, and particle characteristics, without introducing physical probes that may negatively influence the measurement accuracy. In addition, the results obtained by means of laser diagnostics are usually of high spatial and temporal resolution, leading to successful characterization of combustion phenomena. Nowadays, application of laser diagnostics is widespread in combustion and its growing impacts have been evidenced by a number of reviews.[3–6] Among the laser diagnostic methods currently in use for species-specific sensing, a planar laser-induced fluorescence (PLIF) is highly quantitative so that it can yield spatially resolved information. The overviews of PLIF applications, in both fundamental and applied research, have been given[5–8] and they have highlighted its major advantages, such as species specificity, high imaging capacity, and wide applicability.

It is known that the PLIF on OH radicals (OH-PLIF) has become one of the most powerful tools for studies of turbulent combustion. Slightly biased towards the fuel-lean region,[9] the OH peak is located a bit downstream of the CH peak, where the maximum heat release is expected to occur. Accordingly, the OH boundary corresponds to an exothermic reaction zone. It is noteworthy that, although there are various methods to define the flame front location, a common definition is that the location of the peak heat release tends to be approximately coincident with the point of maximum gradient of both temperature and OH concentration distributions. In this sense, the extracted contour from an OH-PLIF image can be regarded as the flame front, as confirmed in numerous studies.[10–13]

Since the detected flame fronts can be used to calculate the critical parameters, such as the flame curvature distributions, and thus allow improvements in the flame surface density (FSD) modeling,[14] enormous efforts have been made in the development of approaches for flame front extraction based on experimentally acquired images. A variety of techniques have been proposed and can be classified into three main categories according to their corresponding levels of complexity.

(i) The simplest approach is to take a signal map of a relevant scalar, such as temperature and chemical species, and to set an appropriate level as a criterion to extract a contour line. The flame front thereby extracted is also called c-derived front since the signal is often normalized as a progress variable c,

†Corresponding author. E-mail: hanyue@sa.buaa.edu.cn

© 2014 Chinese Physical Society and IOP Publishing Ltd

such that it varies between $c = 0$ in the unburned reactants and $c = 1$ in the burned products. It is thus extremely important to select an adequate threshold. When the flame exhibits nearly ideal behavior and the gradient profiles are steep enough to resemble the sharp ramp functions, extracting the contour line at $c = 0.5$[15] is enough to yield good results. From the viewpoint of the gray level, the ideality in this case can be explained by the fact that the histogram has a deep and sharp valley between two peaks representing flames and background, respectively, so that the threshold can be chosen at the bottom of this valley.[16] However, for most real experimental flame images, it is usually not easy to precisely detect the valley bottom. The produced valley even becomes untraceable when it is flat and broad, imbued with noise, or when the two peaks are extremely unequal in height. In order to overcome these difficulties, the valley sharpening technique[17] and the difference histogram method[18] have been proposed, aiming at improving the histogram by making use of information about neighboring pixels in the original image so as to make it efficient and sensible for the threshold selecting. In any event, this class of histogram-based thresholding techniques is largely restricted by the nonidealities, such as excessive background noise in original images and non-linear gradient profiles.

(ii) The next step up in complexity for flame front extraction corresponds to an adaptive thresholding. More advanced statistical analyses on the gray-level histogram are required. Otsu[19] presented a nonparametric and unsupervised method of threshold selection for image segmentation. From the viewpoint of discriminant analysis, an appropriate criterion can be established for evaluating the "goodness" of the threshold. The statistical basis of this procedure simply involves the zero- and first-order cumulative moments of the gray-level histogram. By maximizing the separability of the resultant classes in gray levels, an optimal threshold is automatically derived. Applying the Otsu thresholding algorithm for the optimal threshold setting to a flame image leads to the binarization of the original image into a map of background pixels (unburned reactants) and foreground pixels (burned products). The interface between the burned and the unburned regions can be extracted and considered as the flame front. Otsu's discussion was confined to the elementary case of threshold selection where only the gray-level histogram is sufficient without other a priori knowledge. When dealing with the OH-PLIF images, this method also poses a problem in that the maximum OH concentration across the flame front varies at different locations along the flame front. Significant derivation from the location of the maximum OH gradient may be caused in this case, introducing inaccuracy on a relatively large scale in the flame front extraction. This can raise serious problems about the validity of such techniques, as discussed by Barlow *et al.*[13]

(iii) Instead of directly dealing with the gray-level histogram of the original images, using gradient-based edge detection algorithms turned out to be a more sensible approach to the flame front detection, simply because of its similarity to the definition of the flame front. In fact, the location of a flame front is often taken as the point of maximum OH gradient. Moreover, it is confirmed that the flame front contains OH in super-equilibrium quantities in the reaction zone for both premixed and non-premixed flames,[20,21] which is a beneficial attribute to the class of gradient-based methods for identifying the flame front from OH-PLIF images. In this respect, many variants of edge detection algorithms that has been introduced in the image processing literature[22–25], which were implemented for the flame front detection from the OH-PLIF images[10,26,27]. Among these, the technique proposed by Canny[25] is the most commonly used in the combustion field. In spite of their extensive applications, it is noted that these methods are sensitive to the selection of their operating parameters. Poorly chosen parameters can result in failure of the algorithm or significant inaccuracies. The problem of parameter-dependence on accuracy proved to be particularly pronounced, especially, when attempting to process the large data sets typical of combustion experiments using a single set of parameters selected a priori. In order to improve the robustness of these edge detectors when handling OH-PLIF images with a range of signal-to-noise ratios, Bayley *et al.*[28] demonstrated the ability of their automated data-rejection methods to improve initially identified flame fronts. Specific treatments for isolated curves, spit curves and bridging curves resulting from Sobel edge detector and morphological thinning procedure have been detailed, which include the determination of three more threshold values in addition to two compulsory ones required by Sobel edge detection algorithm. Indeed, the optimization of these threshold values was achieved on a trial-and-error basis by varying these parameters manually and judging the best value based on visual inspection of the test images. For the purpose of minimizing manual work in parameter selection, a statistical method originating in the image processing literature is proposed by Sweeney and Hochgreb.[29] The canny edge detector was nicely combined with Otsu algorithm to obtain an initial flame contour. It is then iteratively evaluated against statistically derived ground truth by a well-defined χ^2 metric,[30] leading to autonomous parameter optimization. Compared to the use of a priori parameters, this auto-evaluation approach using statistical decision procedures is proved to substantially decrease the data rejection rate. However, a potential problem of this method

is the efficiency of parameter search because its performance is highly sensitive to the initial setting. Although parameter search space reduction was introduced to decrease computational cost, the stability, the cost-effectiveness of this purely statistical algorithm and its viability for large data sets remain to be discussed.

The present paper proposes a novel technique for flame front extraction based on the level-set formulation, inspired by the concept originating in medical image processing. The main innovation resides in the block-division strategy and the determination of local adaptive thresholds using an automated routine;: the binarized image sub-regions are used to find initial flame contours which will be optimized through level-set iterations. The rest of this paper is organized as follows: Section 2 briefly introduces the OH-PLIF measurements carried out in this study; Section 3 presents a detailed description of the newly-developed flame front extraction technique, namely Conditioned Level-Set method with Block-division (CLSB method), with examples to visualize how the method is optimized; Section 4 provides evaluation to validate this method; and, concluding remarks are outlined in Section 5 which highlights the advantages of this method.

2. Experimental aspects: OH-PLIF measurements

A schematic diagram illustrating the experimental set-up for OH-PLIF measurements in the current study is shown in Fig. 1.

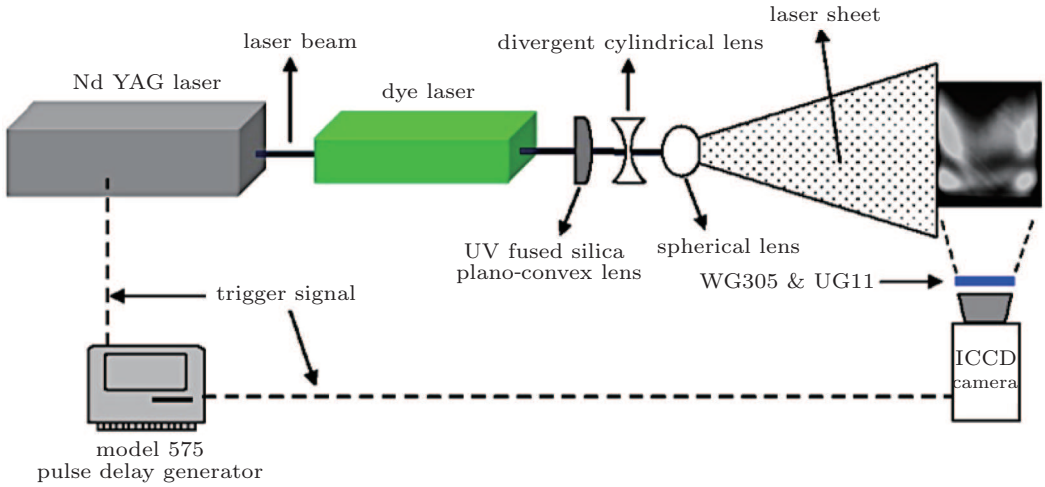


Fig. 1. (color online) Experimental set-up of OH-PLIF system.

A laser system consisting of an Nd:YAG laser (Spectra Physics, Quanta Ray) and a tunable dye laser (Sirah Precision-Scan) is employed to induce fluorescence in OH radicals. High intensity pulse (450 mJ/pulse) is efficiently frequency-doubled in the Nd:YAG laser to generate laser beam at 532 nm, which is used to pump the dye laser operating with Rhodamine 6G dissolved in methanol solvent. The resultant doubled beam is tuned to a wavelength of approximately 282.66 nm. At the exit of the dye laser, the generated laser pulse is measured to be around 20 mJ of energy per shot, with a pulse width of 10 ns.

The laser beam is then shaped into a thin vertical sheet after passing through a series of sheet-forming optics. The present optical arrangement is composed of a UV fused silica plano-convex lens ($f = 1000$ mm), a divergent cylindrical lens ($f = -200$ mm) and a spherical lens ($f = 100$ mm). The cylindrical lens and the spherical lens are served to control the height (~ 56 mm) and the thickness (~ 200 μm) of the laser sheet, respectively.

Thereupon, the created and optimized laser sheet is introduced into the measurement section in order that a spatial map of OH signals can be acquired and recorded with the help of a detection system. In detail, two-dimensional OH fluorescence signals are collected with a UV Nikkor lens (105 mm, $f/4.5$) and focused onto a 16-bit intensified CCD camera (Princeton PI-MAX, 512×512 pixels) in the direction orthogonal to the laser sheet. The ICCD camera is operated with a gating time of 100 ns, and fitted with a combination of WG305 and UG11 filters (Schott glass) so as to reject the undesirable UV wavelength and avoid detection of flame luminosity and spurious light scattering. The current PLIF system affords a field of view of 42.6 mm×42.6 mm. An image scaling of 12.1 pixels/mm is attainable. Triggering and synchronization of the lasers with the ICCD camera is ensured by a digital de-

lay/pulse generator (BNC, model 575).

Concerning the operating conditions, the flames imaged in this study are premixed flames with N_2 dilution, which is stabilized by means of a swirl injector mounted on a cylindrical combustion chamber with an inner diameter of 80 mm. It is found that the obtained OH-PLIF images of premixed flames in diluted regimes are featured with lower than ideal signal-to-noise ratios (SNR). Relatively complex structures of swirling flames lead to significant non-uniformity in OH signal intensity. The magnitude of the maximum OH gradient observed along the flame front can also vary depending on flow or local stoichiometry. After a brief overview of the existing methods for flame front extraction, it can be concluded that the application of conventional methods is limited by low SNRs, as well as the presence of a multiple scales of both OH intensity and OH gradient. Nevertheless, these limitations give an opportunity to evaluate the robustness of the CLSB method, which will be detailed in the following section.

3. Image processing using the CLSB method

The complete CLSB method is composed of three main stages of processing, as follows:

(i) Image pre-processing consists of background subtraction and laser sheet correction (Section 3.2) and anisotropic non-linear diffusion filtering (Section 3.3);

(ii) Initial flame contour identification consists of block-division based on mean flame brush (Section 3.4), self-adaptive threshold setting for sub-region binarization and initial contour extraction using gradient operator (Section 3.5);

(iii) Flame contour optimization using level-set iterative approach with region-lock strategy (Section 3.6).

Figure 2 illustrates the intermediate and final results obtained from the successive steps of the CLSB method described above. It serves as an overview and will be discussed in detail in the following parts of this section.

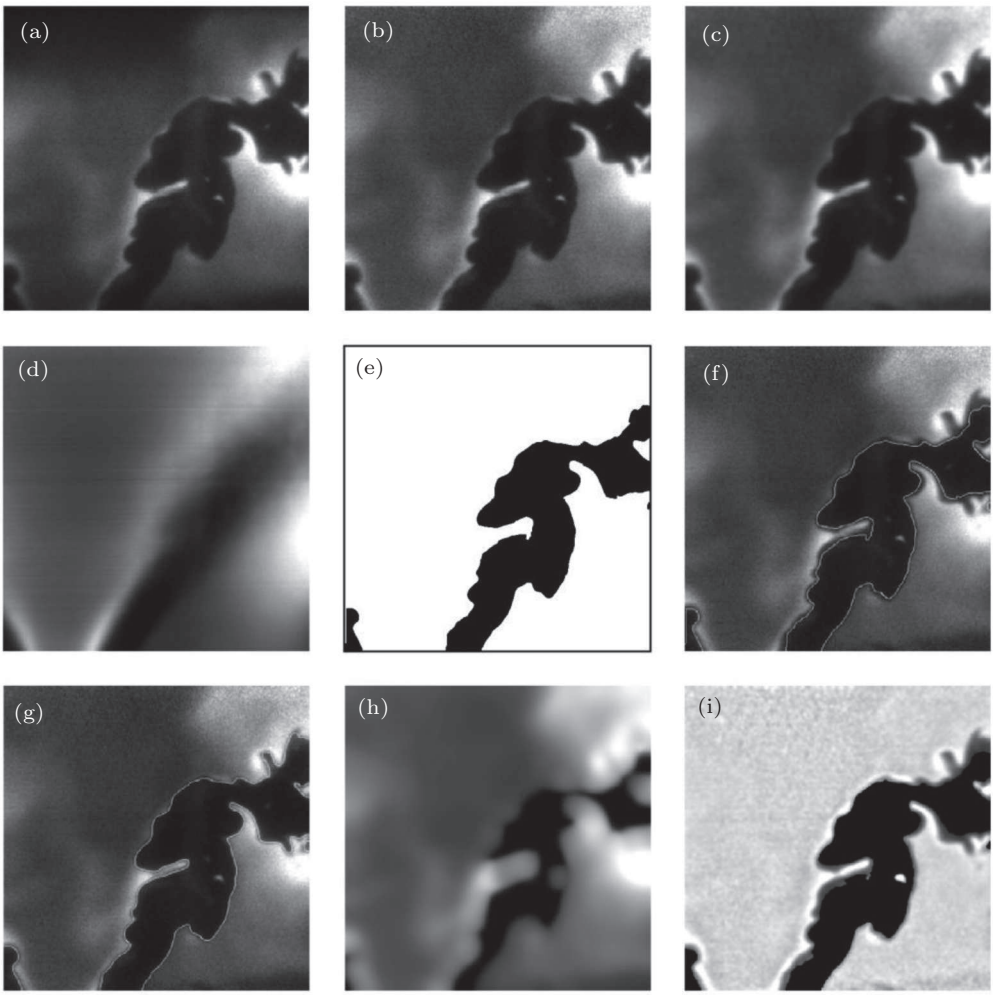


Fig. 2. OH-PLIF image of a sample N_2-diluted methane/air flame showing the successive stages of image processing: (a) raw image; (b) background subtraction and laser sheet correction; (c) anisotropic non-linear diffusion filtering; (d) mean flame brush served to block-division; (e) binarized image based on block-division and local self-adaptive threshold setting; (f) initial flame contour for level-set iteration + original image; (g) final flame contour + original image; (h) final bias flame field; (i) final corrected image without bias and noise.

3.1. Sampling size

For each flame condition, a series of 300 consecutive single-shot PLIF images are recorded to provide a sound basis for analysis. The number of images is not chosen by chance. In fact, a preliminary study on sampling size suggests a dataset of 300 images is sufficient to reduce the statistical uncertainty and optimal to represent flame behavior. The evidence can be found through the statistical analysis. The data from raw images are collected to calculate statistical moments up to the 4th order: mean M1, standard deviation M2, skewness M3, kurtosis M4. Each moment has been normalized relative to the maximum positive peak value for its respective dataset. All the normalized moments that are plotted against the number of data points corresponding to 300 images (Fig. 3) demonstrate a tendency to converge and thus confirm the signal invariance after 300 images.

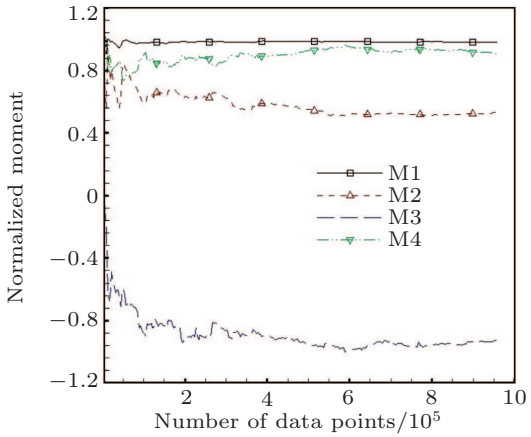


Fig. 3. (color online) Normalized statistical moments (M1: mean; M2: standard deviation; M3: skewness; M4: kurtosis) of the sample flame.

3.2. Background subtraction and laser sheet correction

The irregular nature of the ignition sparks sometimes resulted in dents or cusps in the flame surface. In order to avoid any disturbance during the ignition process, images were captured a relatively long time after ignition. The wall thickness of quartz cylinder (5 mm) is small enough compared to the total diameter of combustion chamber (90 mm) so that aberrations and other distortions present in the optical system become negligible and image de-warping is, thus, not compulsory in this case. Nevertheless, image calibration is still necessary. To achieve this, a calibration plate is placed in the quartz cylinder, of which the front surface is co-planar with the laser-sheet path. After calibration, raw flame image series (Fig. 2(a)) are recorded by an intensified CCD camera, as well as the background images without flame and laser running. Raw experimental data are affected by various factors, including a small temperature dependence and signal quenching, but primarily the presence of noise. In our experiments, the noise in instantaneous images may principally be attributed to random emission associated with the image intensifier inside the camera. The averaged background image is used to correct the raw images from camera and intensifier sensitivity by simple subtraction operation.

Further image pre-processing consists of correcting laser sheet energy profile due to the non-uniformity of the laser sheet that eventually results in the non-uniformity of the signal intensity. For this consideration, acetone is injected and evaporated into the trapped air column at ambient conditions and 300 images of the laser profile obtained with BG39 filter are recorded. With the help of this beam profile compensation scheme, raw images can be corrected by applying the following relation:

$$I_{\text{corrected}} = \frac{I_{\text{raw}} - \bar{I}_{\text{background noise}}}{\bar{I}_{\text{laser profile}} - \bar{I}_{\text{background noise}}}. \quad (1)$$

The result shown in Fig. 2(b) corresponds to raw image from which an averaged background frame of nearly constant level has been subtracted and which has been compensated for laser beam profile variations. It is necessary to rescale the resultant image for further processing. Henceforth, the intensity image ranging from 0 to 65535 (16-bit camera) is converted to double precision ranging from 0 to 1 through linear scaling.

3.3. Anisotropic non-linear diffusion (NLD) filtering

Owing to a limited detector resolution caused by imperfect imaging, OH concentration gradients in the PLIF images are not perfectly sharp. However, the position of the flame contour is of particular interest in the study of turbulent diluted flames. In order to improve the accuracy of flame-front detection, edge enhancement is a highly desirable feature. Traditionally, image smoothing is carried out by convolving the original image with a Gaussian kernel. This operation, from a mathematical point of view, is exactly the same as the solution of the linear diffusion equation with a scalar constant. The high-frequency components of the noise can be efficiently removed by simple smoothing techniques. However, this usually results in image blurring. Perona and Malik[31] proposed to replace the scalar constant with a scalar-valued function which is related to the gradient of the gray-levels in the image. The dependence of the gradient on the differential structure of the image makes the diffusion process non-linear. Since the diffusion coefficient is chosen to vary spatially in such a way as to encourage intra-region smoothing in preference to inter-region smoothing, local edges are enhanced because discontinuities such as boundaries are amplified. Based on the approach originally formulated by Perona and Malik,[31] Malm and Sparr[32] reported the adaptation of anisotropic non-linear diffusion filtering for the enhancement of PLIF images. It is found that the NLD filters demonstrate a good ability to preserve the flame front edges without artificial shifting in position. Motivated by their successful application, the anisotropic NLD filter is chosen for the present study. Numerically, an explicit iterative

scheme was implemented and it was proven to achieve an excellent compromise between computational cost and filter performance. Further information about the formulation of the NLD filtering and a full description of the parameter setting can be found in the literature.[31,32]

As an optimal low-pass filter, Wiener is proven to practically reduce high-frequency pixelation noise as shown in Fig. 4. Smoothing effects in the burned gas region become apparent when increasing the filtering size (Figs. 4(c) and 4(d)). But in the counterpart, one can easily notice the degrading of edge information, leading to difficulties in correctly finding the flame contour. A comparison of the two images (Figs. 2(b) and 2(c)) illustrates several attractive aspects of the NLD filtering process. Clearly, noise levels are drastically reduced without compromising overall intensities. Small structures are preserved as expected. The contour-enhancing properties of NLD filtering are supposed to simplify a successive segmentation of OH boundaries. It can, thus, be concluded that the NLD filtering provides us with adequate smoothing in the burned gas regions and the sharpest flame edge (Fig. 4(b)), which will help to reduce the number of erroneous curves detected by later gradient operations.

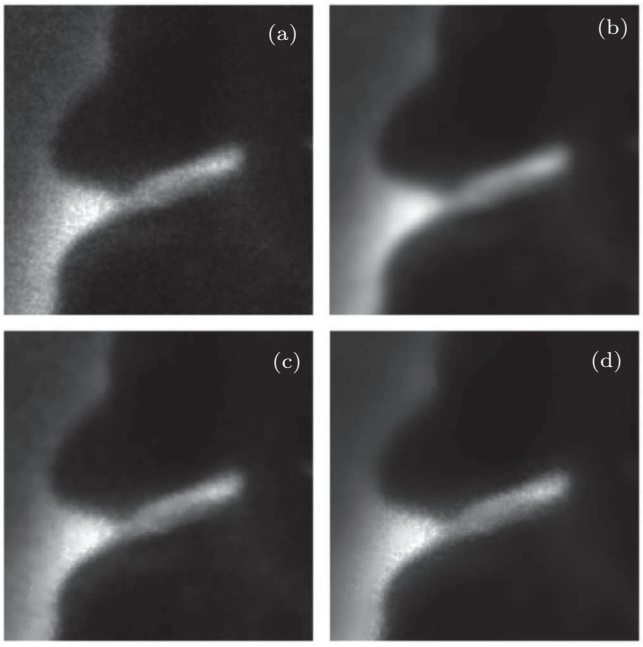


Fig. 4. Filter comparison: (a) PLIF image after background subtraction and laser sheet correction; (b) anisotropic non-linear diffusion filter; (c) Wiener filter [4 4]; (d) Wiener filter [12 12].

3.4. Block-division strategy

Most of the widely employed image segmentation algorithms are region-based and typically rely on the homogeneity of the image intensities in the regions of interest. Due to the intensity inhomogeneity, they often fail to provide accurate segmentation results. Since the OH production is highly nonlinear in nature and is strongly temperature dependent, there are also large-scale variations and associated gradients within regions where OH occurs. Observing the experimentally acquired OH-PLIF images for diluted flames, inhomogeneity of both intensity and gradient make the histogram-based global binarization inappropriate to OH contour identification. After various attempts for flame front detection using diverse existing methods, we found that conventional detectors such as Canny or Sobel edge detector are highly limited when dealing with a complex flame structure. The problem is mainly related to the threshold setting.

As aforementioned, the new processing approach for flame contour extraction introduced in this paper is based on block-division strategy since the structures of swirl-stabilized premixed flames are too complex to be considered as globally uniform. In other words, a global binarization threshold value, even on the basis of histogram study, is far from sufficient. So the idea is to set the local self-adaptive threshold values corresponding to distinct regions after analyzing the mean flame brush. Consequently, block-division is a key step in this method. A major challenge remains in how to achieve a successful block-division by means of a reliable approach that would suit the most types of flames under study. The block size should be neither too small nor too large. If we set a large block size, the intensity variation will be neglected and the threshold values thus calculated in each block no longer give representative local information. If the size is too small, too much emphasis will be put on the local information and the mutual connection among blocks will be ignored, resulting in the detection of isolated erroneous edges inside the burned gas regions.

A robust methodology is provided in the current study. The observation of the heterogeneity of intensity in the averaged flame image (Fig. 2(d)) allows us to automatically set a reasonable block size. Although the concept remains the same, two representative mean flame brushes (Figs. 5 and 6) are examined. The determination of block size is closely relevant to the intensity profiles in both x and y directions. The idea is to capture all the dramatic changes in intensity with a least number of blocks. In Fig. 5, a mean flame brush with the presence of the corner recirculation zone (CRZ) is analyzed in terms of intensity. The intensity profile in horizontal direction possesses two notable modes. Accordingly the characteristic length corresponding to the minimum length to include unique mode in a block can be deduced. In this case, this characteristic length is measured to be around 57 pixels in horizontal direction, and 128 pixels in vertical direction. Consequently, the block size should be set to 57×128. It is noteworthy that the final block size should be determined by avoiding marginalization effect. More concisely, in a 512×512 flame image, if the characteristic length is around 57, we should first make a simple calculation before taking this value as block size:

$512/56 = 9.1$, while $512/57 = 8.98$, which means if $x = 56$, we will have nine identical blocks and a very small block leading to unexpected marginal effect; but if $x = 57$, we will get eight equally-sized blocks plus a slightly smaller block, and since the difference is negligible, it has no reason to negatively influence further calculations.

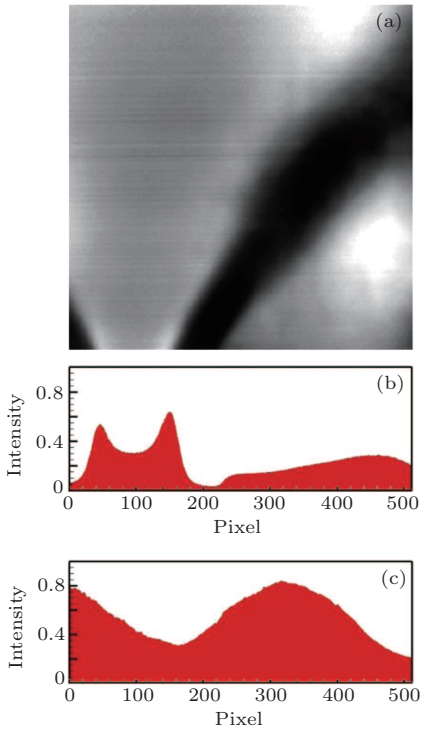


Fig. 5. (color online) (a) Mean flame brush with corner recirculation zone (CRZ); (b) OH intensity profile in the x axis; and (c) OH intensity profile in the y axis.

A similar approach can be applied to mean flame brush where no CRZ appears (Fig. 6). The intensity profiles are relatively simple in this case, thus a block size of 103×256 is large enough to take all the variations into account.

It is of crucial importance to point out that the CLSB algorithm is completely autonomous. The most critical parameter is the block size, which is determined automatically after analyzing the mean flame brush image. With the input image, the line of greatest changes in intensity corresponding to the maximum standard deviation is tracked. After examining the intensity profile of this line and considering the mode uniqueness and marginalization effect, a set of block size will be provided. It is confirmed that a single value of block size is sufficient to produce satisfactory results for nearly all images processed within an experimental run. The different operating conditions which present similarity in mean flame brushes might share the same setting of block size.

In terms of execution time, the nature of block-division renders parallelization of the algorithm possible. With a typically four-core PC, a speedup of 3.33 is attainable. This is particularly useful when dealing with a considerable number of images, since the execution time will be largely reduced.

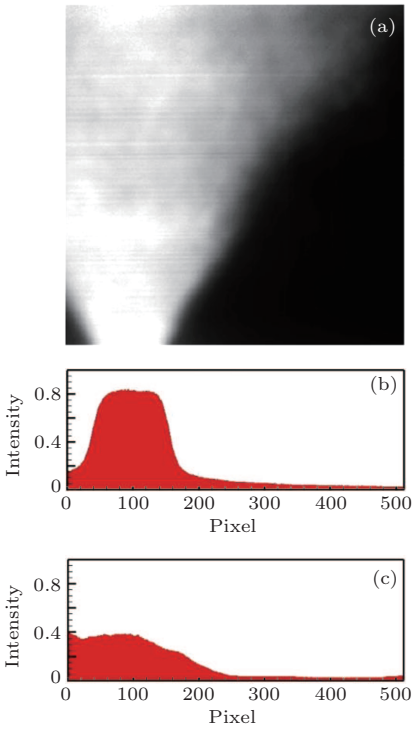


Fig. 6. (color online) (a) Mean flame brush without corner recirculation zone (CRZ); (b) OH intensity profile in the x axis, and (c) OH intensity profile in the y axis.

3.5. Self-adaptive threshold setting for binarization

As a good approximation, the flame front lies close to the region where maximum gradient of the OH concentration is observed. The ideal behavior of OH concentration and its gradient profile across the flame front has been plotted by Sweeney *et al.*[29] The OH concentration rises from zero in the unburned gas to a peak within the flame front, relaxing down to the equilibrium concentration. Due to the complex physical phenomena that may be involved in the diluted swirling flames, non-ideality should be accounted for. A typical 3D representation of intensity gradients is presented in Fig. 7. The magnitude of the maximum gradient observed along the flame

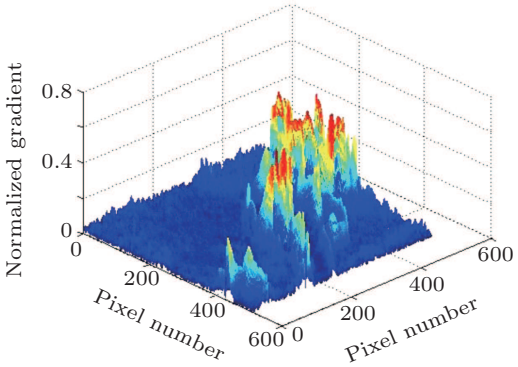


Fig. 7. (color online) 3D representation of global gradient for the sample flame.

front varies depending on flow or local stoichiometry. This implies that a single threshold value could generate inaccuracies or even complete failure in edge detection. The advantage of block-division is thus verified.

Once the block size is set, each instantaneous image can be divided into blocks (Fig. 8). The block index can be expressed in the form of (*yi*, *xi*), similar to an element in a matrix. Self-adaptive threshold values are then calculated inside each block. In most research, the threshold value is set manually and only one type of threshold, either gradient or intensity, is taken into consideration. We aim at setting the self-adaptive threshold with least manual adjustment so as to make the computational approach more efficient. The idea is to make use of both gradient and intensity information given by the PLIF image.

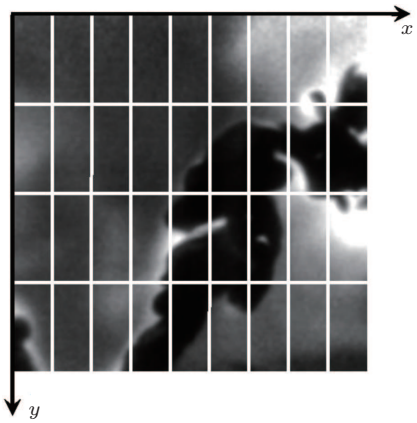


Fig. 8. Block-division representation of the sample flame (a 9×4 matrix), block index from (1, 1) – up left to (4, 9) – down right.

Firstly, we calculate the intensity gradient inside each block and determine the gradient threshold by the concept of dimensionality reduction (from 2D to 0D). In detail, it is noticed that the variation in the gradient is enormous in the *y*-axis direction inside most blocks since it is the main direction of flame propagation. In contrast, little variation is observed in the *x*-axis direction inside each block. In order to reserve the representative information of the flame, we first look for the maximum in each line of the *x* axis, and then calculate the average of these maximum values in the *y*-axis direction. So far, each block has a specific gradient threshold value (0D) deduced from gradient information in both *x* and *y* direction (2D). The gradient threshold values are not used directly as local threshold. On the contrary, they are served to calculate the weight of each gradient threshold over the maximum threshold among them (Table 1).

Secondly, the intensity threshold is determined by iterative dichotomization. We look for the maximum and minimum intensity and calculate their average, denoted by T. All the pixels possessing a larger intensity than T are sorted to calculate a new average (T_1), so are all the other pixels (T_2). Then, we calculate the average of T_1 and T_2, and compare it with the initial average T. If the difference is larger than the convergence criterion, which is set to be 1×10^{-4}, the iteration is re-launched. The iterative procedure will not be ceased until the convergence condition is attained. The results are shown in Table 2.

Table 1. Local gradient weight (W) of the sample flame.

x	1	2	3	4	5	6	7	8	9
$y=1$	0.3369	0.3368	0.3359	0.3356	0.3350	0.3497	0.3463	0.3910	0.4656
$y=2$	0.3380	0.3344	0.3338	0.3333	0.5218	0.3830	0.6141	0.6620	0.5926
$y=3$	0.3355	0.3340	0.3368	0.5429	0.7297	0.3976	1	0.3553	0.6155
$y=4$	0.8819	0.3355	0.3719	0.8865	0.7084	0.3916	0.4332	0.3365	0.3375

Table 2. Local intensity threshold (I) of the sample flame.

x	1	2	3	4	5	6	7	8	9
$y=1$	0.2452	0.2126	0.1991	0.1763	0.1832	0.3085	0.4516	0.5747	0.4085
$y=2$	0.3205	0.2370	0.1869	0.1704	0.0864	0.0856	0.1490	0.2941	0.1836
$y=3$	0.2350	0.2037	0.2453	0.3385	0.2421	0.1779	0.1594	0.4798	0.6100
$y=4$	0.2571	0.2171	0.2893	0.1883	0.0939	0.1283	0.1338	0.2385	0.2350

Finally, we propose a definition to self-adaptive threshold for each block in the following expression: $\mathrm{SAT} = I \times W$, with the SAT denoting the self-adaptive threshold, I the intensity threshold, W the gradient weight, which is shown in Table 3. The originality of this idea is to use gradient weight to correct intensity threshold. By linking the gradient with the intensity, the obtained local self-adaptive threshold is based on the relatively complete information of each block. In the block (2,6), low intensity ($I = 0.0856$) is observed with a small gradient weight ($W = 0.3830$), leading to the minimum local self-adaptive threshold (SAT=0.0328). In contrast, the maximum local self-adaptive threshold (SAT=0.3755) is found in block (3,9), which results from high intensity ($I = 0.6100$) and moderate gradient weight ($W = 0.6155$). Due to the complexity of the flame structure, the level of the gradient weight is not always in agreement with that of the intensity. For exam-

ple, block (3, 7) and (3, 8) are at a similar level in terms of local self-adaptive threshold, but their individual information is quite the opposite. The sharpest gradient ($W = 1$) lies in block (3, 7), but the low intensity level ($I = 0.1594$) forces the final threshold value (SAT=0.1594) to be much smaller. On the contrary, the high intensity ($I = 0.4798$) in block (3, 8) is weakened by a less steeper gradient ($W = 0.3553$), giving a medium value of final threshold (SAT=0.1704).

Table 3. Local self-adaptive threshold (SAT) of the sample flame.

x	1	2	3	4	5	6	7	8	9
$y = 1$	0.0826	0.0716	0.0669	0.0592	0.0614	0.1079	0.1564	0.2247	0.1902
$y = 2$	0.1083	0.0793	0.0624	0.0568	0.0451	0.0328	0.0915	0.1947	0.1088
$y = 3$	0.0788	0.0680	0.0826	0.1838	0.1766	0.0707	0.1594	0.1704	0.3755
$y = 4$	0.2267	0.0728	0.1076	0.1669	0.0665	0.0502	0.0580	0.0802	0.0793

With the obtained local threshold settings, the previous image can easily be binarized (Fig. 2(e)). After applying a simple gradient operator to the binarized image, we are able to extract the flame contour (Fig. 2(f)), which approximately follows the flame shape. Nevertheless, the obtained contour has failed to stick precisely to the original flame front. Some errors still remain evident if we take a close look. This initiates the application of level-set iterative method.

3.6. Level-set method: Background theory, numerical implementation and optimization

The level-set method, which was originally used as numerical technique for tracking interfaces and shapes, has been increasingly applied to image segmentation in the past decade.[33–37] A more straightforward definition of level-set is the set of points that have same function value. Li *et al.*[36] proposed a variational level-set approach which does not rely on the assumption of intensity homogeneity. By deriving a local clustering criterion function for the image intensities in a neighborhood of each point and integrating with respect to the neighborhood center, an energy functional can be defined and converted to a level-set formulation, as shown below:

$$F = \varepsilon + \nu L + \mu R, \tag{2}$$

where F is the energy functional; ε is the data term; L serves to regularize the zero level contour by penalizing its arc length;[35,36] R serves to regularize the entire level-set function by penalizing its deviation from signed distance;[37] ν and μ are two parameters to be fixed. By minimizing this energy, the results of image segmentation given by the level-set function can be obtained. The steepest descent strategy for finding minima of the energy function consists of starting from some initial state, and then changing the state iteratively following the opposite of the gradient vector. In this framework, an initial function must be constructed such that its zero level set corresponds to the position of the initial contour. Mathematically, the standard gradient descent method involves solving the gradient flow equation. Details about the fundamental level-set formulations and energy minimization are described by Li *et al.*[38]

An interesting aspect of level-set method is the description of the image model, in which intensity inhomogeneity is attributed to a component of an image. Segmentation and bias correction can, thereby, be unified within a single framework. We consider the following multiplicative model,[36] in which the observed image can be modeled as

$$I = bJ + n, \tag{3}$$

where I is the measured image intensity, J is the true image to be restored, b is the component that accounts for the intensity inhomogeneity, and n is additive noise (in Fig. 2, image $C =$ image $H \times$ image I). The component b is referred to as a bias field and it is generally assumed to be slowly varying. The true image J measures an intrinsic physical property of the objects being imaged, which is therefore assumed to be piecewise (approximately) constant. The additive noise is usually assumed to be zero-mean Gaussian noise. This interpretation will be used to assess the application of level-set method in the following part (Fig. 9). As a result, the level-set method is able to simultaneously segment the image and estimate the bias field. The estimated bias field can be used for intensity inhomogeneity correction (or bias correction).

Concerning the numerical implementation, a central difference scheme along with Neumann boundary condition has been implemented to solve the gradient flow equation. Since the model used in this paper is not sensitive to the choice of the parameters, all experimental data can be processed successfully with the fixed parameters, as follows: $\mu = 1.0$, $\nu = 0.001 \times 255^2$, $\Delta t = 0.1$. The default setting of ν is due to the image rescaling after filtering so that the intensity range lies in [0, 255]. At each time step, the constant and the bias field are updated, which requires computing a total of four convolutions during curve evolution. The convolution kernel K is constructed to be a 45×45 mask, which is used as an optimal setting in our application. The convergence of the re-

sults is sufficiently attained after 18 steps of iteration for all the cases.

In general, the level-set methods are quite sensitive to contour initialization. Considering the specific features of the flame images, in place of arbitrary initial contours, the binarized image (Fig. 2(e)) that resulted from block-division and local self-adaptive threshold setting is intentionally used to initiate the level-set approach. With this conditioned initialization strategy, the calculations can easily be converged: both segmentation accuracy and efficiency are improved.

It is believed that one can make use of the flame contour detected from OH-PLIF images to identify the burned and unburned zones. However, the block-division strategy is found to globally underestimate the local threshold levels so that the extracted contour is slightly shifted downstream the unburned zone (Fig. 2(f)). Owing to this characteristic, the unburned region in the binarized image (initialization) is assigned -1 (black) constantly during the iterative level-set calculations; only the initial burned region (white) would take part in the iteration. Consequently, unnecessary calculations are avoided and the continuity of the unburned region is guaranteed by the proposed region-lock optimization. The final flame contour is superimposed on the raw image (Fig. 2(g)).

It is necessary to emphasize the importance of the combination of block-division strategy and level-set approach in the CLSB method. The results compared in Fig. 9 are strong evidence to suggest that the direct use of level-set iterative formulation without local block treatments is not satisfactory (Fig. 9(a)) since the initialization has not been improved. The corresponding bias field is seriously deformed (Fig. 9(b)) resulting in a total error in final corrected image (Fig. 9(c)). When the level of the gradients varies significantly across the image, the level-set scheme with arbitrary initialization proves to be insufficient to obtain a correct multi-scale segmentation. In this case, applying block-division and local threshold setting provides the optimal initial condition with success for detecting flame fronts using level-set method. While the block-division is the core of the CLSB method, level-set iteration is also compulsory to improve the accuracy of the results. It is apparent that level-set iteration is efficient to deal with the details along the flame contour (Fig. 10(c)). The superior performance of the level-set method can be explained partially by the fact that the image is pre-processed by an anisotropic NLD filter. From a mathematical point of view, with level-set methodology, edge detection process is performed by the minimization of an energy function, which is the sum of two terms: the a priori term and a term depending on the data available. It is shown that the approximation of anisotropic diffusion may be seen as a gradient decent of the a priori part of the energy function.[31] The side effect of NLD filtering is thereby the improvement of energy minimization in the preliminary stage.

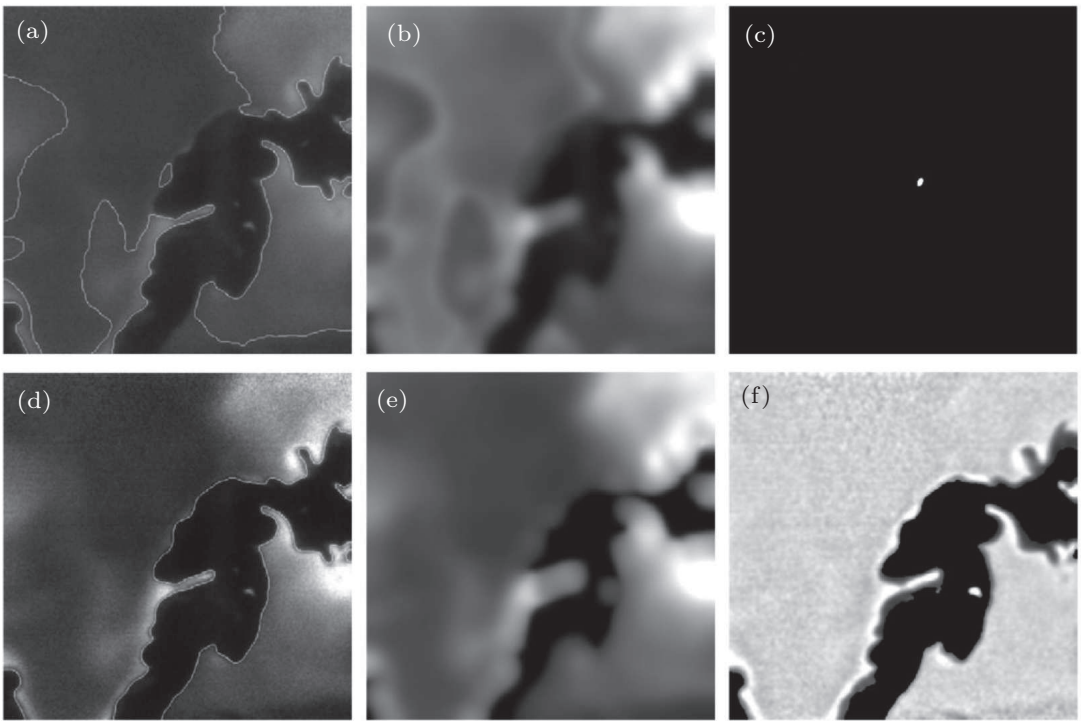


Fig. 9. Level-set method without block-division: (a) final flame contour + raw image; (b) final bias flame field; (c) final corrected image without bias and noise. Level-set method with block-division: (d) final flame contour + raw image; (e) final bias flame field; (f) final corrected image without bias and noise.

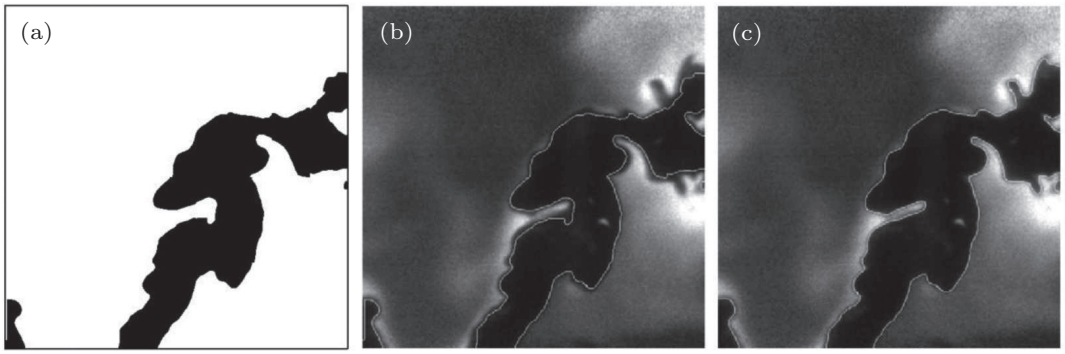


Fig. 10. (a) Binarized flame image; (b) block-division without level-set iteration; (c) block-division with level-set iteration.

4. Evaluation of the CLSB method

In the domain of combustion image processing, quantitative evaluation of the performance of segmentation techniques lacks consensus in the literature, which impedes the unambiguous evaluation of flame front location. Generally, the quantitative merits of a given edge detection algorithm have not been addressed. This is unsatisfactory in studies where the accurate mapping of the flame front is of particular importance, such as the determination of scalars at the flame front. Several methods of quantitative comparison dependent on the use of a ground truth (GT) have been proposed.[39–44] In these studies, either synthetic images or human-derived ground truths (HDGTs) have been used as a reference against which to evaluate the output of a given edge detection scheme. Using synthetic images provides an objective basis without any human interference[9,41,43,44] since the location of maximum gradient can be explicitly defined in advance. However, even though this approach enables definitive GTs, it is difficult to create complicated synthetic images similar to real world applications. HDGT methods are attractive because quantitative evaluation is grounded in the experimental images rather than simple synthetic images. These approaches raise issues of human error and bias when extracting edge locations manually[40,42] In a case where the gradients are strong enough and the SNR is relatively high, the flame contour may be extracted by hand with limited accuracy. However, this may not be feasible in the case of low SNRs or flames with weak gradients. Yitzhaky and Peli[30] develop an evaluation method which does not rely on synthetic images or HDGTs. A χ^2 metrics is defined to generate a statistically derived ground truth (SDGT) autonomously from experimental images. SDGTs are advantageous to provide objective reference directly based on experimental data, but they are time-consuming which restricts their application to small area of experimental images.

In this paper, the robustness of the CLSB method has been assessed in terms of noise sensitivity against definitive GTs (Section 4.1). Among the simplest synthetic images, a circle is chosen since its curvature can be specified in its creation. This facilitates comparisons of curvature distributions because the reference is unambiguous. Due to the complicated flame structures, it is impossible to extract flame contours manually with confidence. As a result, the evaluation on the accuracy of the CLSB method has been carried out through real experimental flame images with the help of the derived SDGT (Section 4.2).

4.1. Evaluation against GT

As aforementioned, a circle with specified curvature ($H = 0.0286\ \text{mm}^{-1}$) is generated as GT. The ideal binary image (Fig. 11(a)) is superposed with Gaussian noise of different levels derived from the OH signals and scaled to achieve different levels of noise (Figs. 11(b)–11(d)). Intensity inhomogeneities are also added.

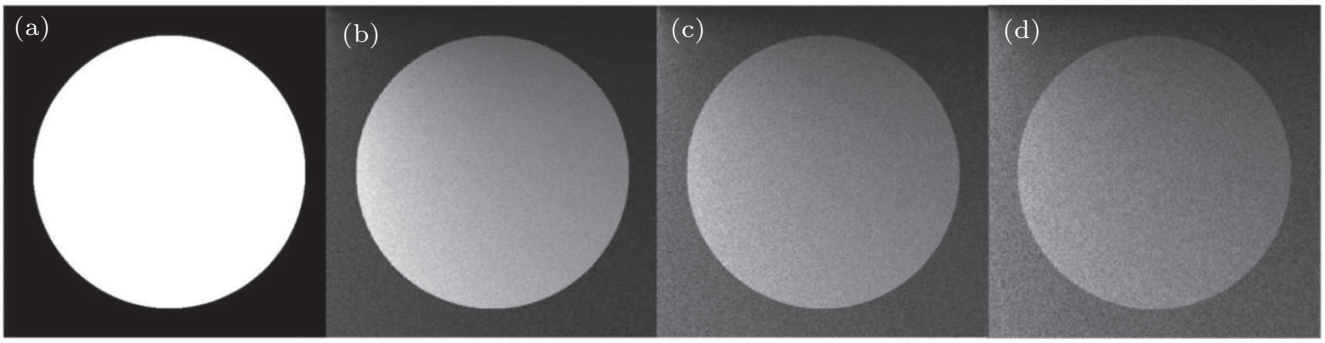


Fig. 11. Ground truth (GT) circles added with intensity inhomogeneities and Gaussian noise: (a) reference circle; (b) SNR = 10; (c) SNR = 4; (d) SNR = 3.

After applying the CLSB method, the extracted contours are used to calculate the curvature distribution. It is noticed from Fig. 12 that when the SNR is as high as 10, the curvature distribution abides by the Dirac delta function, centered at the reference curvature. As the SNR falls to 4, the Dirac distribution is still well followed around the reference curvature, while the variance tends to increase. When the SNR reaches 3, the curvature distribution is a little distorted and its center is shifted to the left of the reference curvature. The variance is much higher than that of the previous cases. The accuracy is degraded accordingly. The circle test provides proof that the CLSB method is robust to the intensity inhomogeneity as well as to the noise sensitivity. For simple synthetic images with the presence of high-level noise, this method demonstrates good ability to maintain high accuracy.

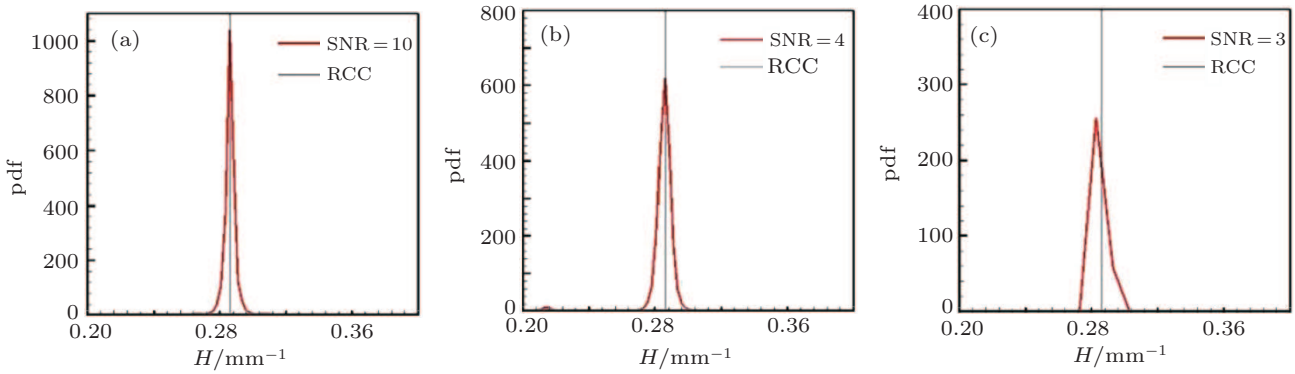


Fig. 12. (color online) Circle test results: curvature distributions (pdf: probability density function; H: curvature) in comparison to reference circle curvature (RCC=0.0286): (a) SNR = 10; (b) SNR = 4; (c) SNR = 3.

4.2. Evaluation against the SDGT

The addition of N_2 as diluents into the reactants lowers the flame temperature efficiently, leading to a notable decrease in OH signal compared to that of the non-diluted flames. The experimental images used throughout the analysis in this paper present a range of SNRs corresponding to different operating conditions, which enables a complete comparison of the robustness to noise sensitivity and flame topology. Examples of instantaneous flame images with extracted flame contour are given in Fig. 13.

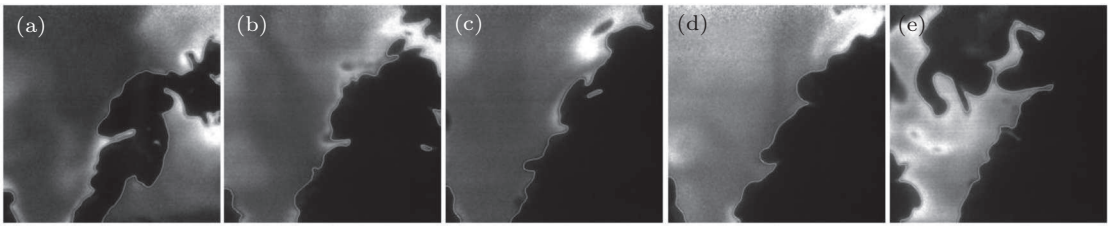


Fig. 13. Instantaneous images of diluted swirling flames with extracted flame contour: (a) SNR = 7.9; (b) SNR = 9.8; (c) SNR = 10.1; (d) SNR = 13.2; (e) SNR = 12.4.

The SNR in the experimentally acquired images was calculated by selecting a background region in the unburned zones and an equally sized signal region in the burned zones. The intensity values in these regions were used to calculate the SNR[26]

$$\mathrm{SNR} = \frac{\mu_{\mathrm{signal}} - \mu_{\mathrm{background}}}{\sigma_{\mathrm{signal}}}. \tag{4}$$

As the geometry of the flame varies from shot to shot, these regions have to be specified manually for each image. Using a subset of 30 experimental images for each operating condition, the mean SNR was determined and found to vary from 6.1 to 13.6.

In this paper the image rejection rate is calculated on the basis of each experimental run. Although the algorithm proposed by Sweeny *et al.*[26] to obtain a SDGT contour based on real experimental dataset is poorly cost-effective, the precision of a such method is guaranteed. For this reason, their algorithm is adopted in this study to derive SDGT contours of OH-PLIF flame images. The SDGT contours are served to evaluate the accuracy of the CLSB method. An objective judgment is performed with the help of a contour-based metric e_{mean}, namely, mean localization error,[38]

$$e_{\mathrm{mean}}(C) = \frac{1}{N}\sum_{n=1}^{N} \mathrm{dist}(P_i, S), \tag{5}$$

where C is the extracted contour; S is the accurate contour given by the SDGT; P_i, $i = 1$, N is the point on the contour C. The distance from the point P_i to the SDGT contour S is thus computed to obtain the deviation from the contour C to the contour S.

Since accuracy is desired in this study, the critical value of e_{mean} is set to be lower than 0.4 pixels. All the images where e_{mean} exceeds 0.4 will be rejected. The recorded image rejection rate is plotted against the SNR in Fig. 14. The results indicate that for images with the SNR as low as 7, the CLSB method still has an acceptable performance (rejection rate is 0.2). When the SNR surpasses 8, only about 10% images would be rejected. This analysis, which is based on real experimental data of OH-PLIF flame images, confirms the outstanding performance of the CLSB method concerning its robustness to noise sensitivity and flame topology.

The newly-developed CLSB method is compared with other alternative edge detection operators (Fig. 15). The attempts to apply the widely-used edge detectors on the sample flame from this study were not successful. It is worth noting that all the appropriate pre-processing steps previously described (background subtraction, laser sheet correction, and NLD filtering) are completed prior to applying these edge detectors in order to reach a fair comparison. Evidently, the noise content was poorly handled in the post-flame gases, which produced erroneous flame fronts (Figs. 15(a) and 15(b)). The discontinuity as well as the localization error at the edges of flame front remains apparent (Figs. 15(c)–15(e)). Processing the sample flame with the CLSB method is shown to have noticeable benefits on the flame front detection (Fig. 15(f)) and it outperformed the other techniques. The erroneous curves are eliminated and the localization precision is achieved. The fully burned gas region is correctly identified. Further evidence can be provided by the estimation of the mean localization error. Figure 16 demonstrates that the CLSB method is able to yield a substantially decreased localization error as compared to the Sobel detector. In addition, the level-set iteration also contributes significantly to improvements in the precision of the contour localization when compared to the approach of only involving a block-division strategy.

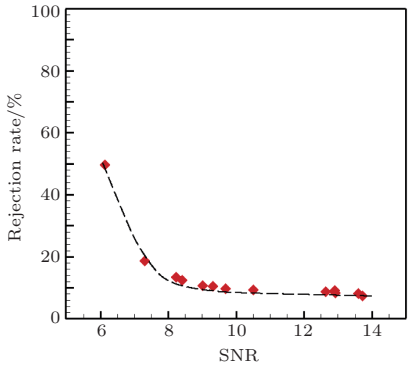


Fig. 14. (color online) Percentage of images rejected using CLSB method at various SNR levels (diamond: experimental data; dashed line: tendency curve).

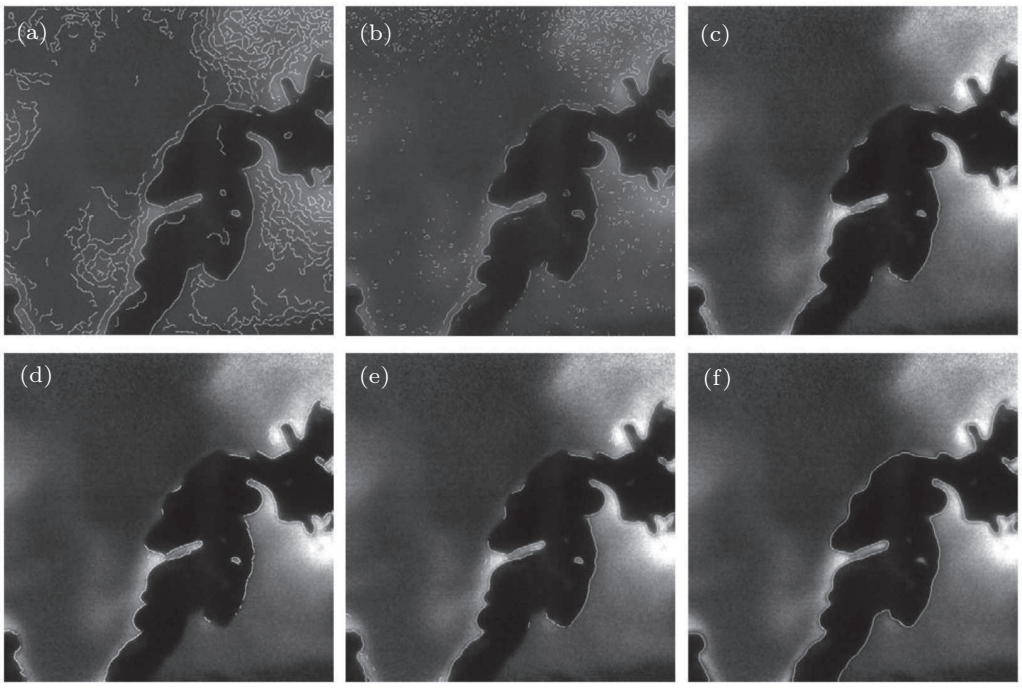


Fig. 15. Edge detector comparison: (a) Canny edge detector; (b) log edge detector; (c) Prewitt edge detector; (d) Roberts edge detector; (e) Sobel edge detector; (f) CLSB method.

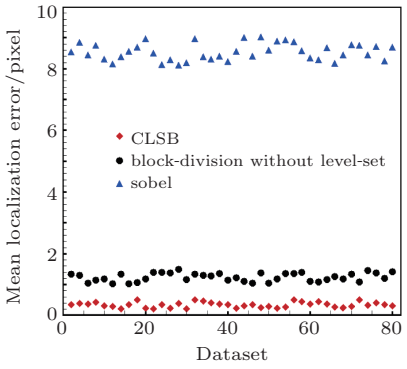


Fig. 16. (color online) Mean localization error of experimental datasets using three different approaches (delta: sobel detector; circle: block-division without Level-set; diamond: CLSB method).

5. Conclusions

The OH-PLIF images of diluted premixed flames are featured with lower-than-ideal SNRs, significant spatial non-uniformity in signal intensity, an extensive range of the maximum gradients observed along the flame front, weak boundary, and complex flame topology. In this context, processing a large set of data with least manual adjustment becomes more challenging. A totally autonomous method (CLSB) for flame front identification is developed where the only inputs are the raw instantaneous images that are directly obtained from OH-PLIF measurements and the corresponding mean flame brush image. The originalities and advantages of the CLSB method are outlined below.

(i) With the original block-division strategy and the corresponding iterative procedure for local threshold value calculation, the inputs of the algorithm only involve the block size, which is automatically determined by preliminary statistical analysis on mean flame brush image. All of the other parameters and the final self-adaptive threshold values will be calculated autonomously in massive quantities without manual adjustment for each image.

(ii) The accuracy of the contour extraction procedure is guaranteed by the level-set iterative calculation. The conditioned initialization and region-lock optimization show benefits when using the level-set formulation. The image model description is also helpful to results assessment.

(iii) Comparisons with traditional edge detection operators demonstrate the superior performance of the CLSB method in terms of robustness to noise sensitivity and accuracy. With a range of flame conditions tested, this method shows high efficiency for post-processing of low SNR images, thus is perfectly adapted to deal with OH-PLIF images of diluted flames.

(iv) The algorithm is convenient to be parallelized regarding its block-division specificity, thus having the potential to make the calculation more rapid and cost-effective.

(v) This method is quite general: a straightforward extension to multi-thresholding problems is feasible owing to block-division strategy; the algorithm is readily to be applied to the post-processing of images obtained from other planar laser diagnostics.

References

[1] Chen D, Liu W Q, Zhang Y J, Liu J G, Wei Q N, Kan R F, Wang M, Cui Y B and Chen J Y 2006 *Chin. Phys. Lett.* **23** 2446
[2] Xu Z Y, Liu W Q, Liu J G, He J F, Yao L, Ruan J, Chen J Y, Li H, Yuan S, Geng H and Kan R F 2012 *Acta Phys. Sin.* **61** 234204 (in Chinese)
[3] Wolfrum J 1998 *Proc. Combust. Inst.* **27** 1
[4] Kohse-Hoinghaus K, Barlow R S, Alden M and Wolfrum J 2005 *Proc. Combust. Inst.* **30** 89
[5] Eckbreth A C 1996 *Laser Diagnostics for Combustion Temperature and Species* (2nd Edn.) (UK: Gordon and Breach)
[6] Kohse-Hoinghaus K and Jeffries J B 2002 *Applied Combustion Diagnostics* (New York: Taylor and Francis)
[7] Kohse-Hoinghaus K 1994 *Prog. Energy Combust. Sci.* **20** 203
[8] Daily J W 1997 *Prog. Energy Combust. Sci.* **23** 133.
[9] Pfadler S, Beyrau F and Leipertz A 2007 *Opt. Express* **15** 15444
[10] Hartung G, Hult J, Kaminksi C F, Rogerson J W and Swaminathan N 2008 *Phys. Fluids* **20** 035110
[11] Hassel EP and Linow S 2000 *Meas. Sci. Technol.* **11** R37
[12] Ayoola B O, Balachandran R, Frank J H, Mastorakos E and Kaminski C F 2006 *Combust. Flame* **144** 1
[13] Barlow R S, Wang G H, Anselmo-Filho P, Sweeney M S and Hochgreb S 2009 *Proc. Combust. Inst.* **32** 945
[14] Veynante D, Piana J, Duclos J M and Martel C 1996 *Proc. Combust. Inst.* **26** 413
[15] Gashi S, Hult J, Jenkins K W, Chakraborty N, Cant S and Kaminski C F 2005 *Proc. Combust. Inst.* **30** 809
[16] Prewitt J M S and Mendelsolhn M L 1966 *Ann. Acad. Sci.* **128** 1035
[17] Weszka J S, Nagel R N and Rosenfeld A 1974 *IEEE Trans. Comput.* **C-23** 1322
[18] Watanabe S and CYBEST Group 1974 *Comp. Graph. Image Process.* **3** 350
[19] Otsu N 1979 *IEEE Trans. Syst. Man. Cybern.* **9** 62
[20] Bechtel J H and Teets R E 1979 *Appl. Opt.* **18** 4138
[21] Drake M C, Pitz R W, Lapp M, Fenimore C P, Lucht R P, Sweeney D W and Laurendeau N M 1984 *Proc. Combust. Inst.* **20** 327
[22] Roberts L G 1965 *Optical and Electro-Optical Information Processing* (Cambridge: MIT Press) p. 159
[23] Prewitt J M S 1970 *Picture Processing and Psychopictorics* (Waltham: Academic Press) p. 75
[24] Sobel I 1970 *Camera Models and Machine Perception* (Ph.D. dissertation) (Stanford: Stanford University)
[25] Canny J F 1986 *IEEE Trans. Pattern Anal. Mach. Intell.* **8** 679
[26] Sweeney M S, Hochgreb S, Dunn M J and Barlow R S 2011 *Proc. Combust. Inst.* **33** 1419
[27] Boxx I, Stohr M, Carter C and Meier W 2010 *Combust. Flame* **157** 1510
[28] Bayley A E, Hardalupas Y and Taylor A M P K 2012 *Exp. Fluids* **52** 963
[29] Sweeney M and Hochgreb S 2009 *Appl. Opt.* **48** 3866
[30] Yitzhaky Y and Peli E 2003 *IEEE Trans. Pattern Anal. Mach. Intell.* **25** 1027
[31] Perona P and Malik J 1990 *IEEE Trans. Pattern Anal. Mach. Intell.* **12** 629
[32] Malm H and Sparr G 2000 *J. Opt. Soc. Am. A* **17** 2148
[33] Caselles V, Catte F, Coll T and Dibos F 1993 *Num. Math.* **66** 1
[34] Malladi R, Sethian J A and Vemuri B C 1995 *IEEE Trans. Pattern Anal. Mach. Intell.* **17** 158
[35] Chan T and Vese L 2001 *IEEE Trans. Image Process.* **10** 266
[36] Li C, Huang R, Ding Z, Gatenby J C, Metaxas D N and Gore J C 2008 *Proc. Med. Image Comput.* **5242** 1083
[37] Li C, Xu C, Gui C and Fox M D 2010 *IEEE Trans. Image Process.* **19** 3243
[38] Li C, Huang R, Ding Z, Gatenby J C, Metaxas D N and Gore J C 2011 *IEEE Trans. Image Process.* **20** 2007
[39] Peli T and Malah D 1982 *Comput. Graph. Image Process.* **20** 1
[40] Heath M, Sarkar S, Sanocki T and Bowyer K 1998 *Comput. Vision Image Understand.* **69** 38
[41] Venkatesh S and Kitchen L J 1992 *CVGIP: Graph. Models Image Process.* **54** 23
[42] Hoover A, Jean-Baptiste G, Jiang X, Flynn P J, Bunke H, Goldof D and Bowyer K 1996 *IEEE Trans. Pattern Anal. Mach. Intell.* **18** 673
[43] Zhang Y J 1996 *Pattern Recogn.* **29** 1335
[44] Román R, Gómez-Lopera J F, Atae-Allah C, Martínez-Aroza J and Luque-Escamilla P L 2001 *Pattern Recogn* **34** 969